ELSEVIER

J. Non-Newtonian Fluid Mech. 153 (2008) 53–61

Journal of Non-Newtonian Fluid Mechanics

www.elsevier.com/locate/jnnfm

Enhancement of velocity contrasts by shear-thinning solutions flowing in a rough fracture

H. Auradou [b], A. Boschan [a,b], R. Chertcoff [a], S. Gabbanelli [a], J.P. Hulin [b,*], I. Ippolito [a]

[a] *Grupo de Medios Porosos, Facultad de Ingeniería, Universidad de Buenos Aires, Paseo Colón 850, 1063, Buenos-Aires, Argentina*
[b] *Univ Pierre et Marie Curie-Paris6, Univ Paris-Sud, CNRS, F-91405 Lab FAST, Bat 502, Campus Univ, Orsay, F-91405, France*

Received 19 February 2007; received in revised form 24 October 2007; accepted 28 November 2007

Abstract

Flow and transport are studied in transparent model fractures with rough complementary self-affine walls with a relative shear displacement $\vec{u}$. The aperture field is shown to display long range correlations perpendicular to $\vec{u}$: for flow in that direction, the width and geometry of the front of a dyed shear-thinning polymer solution displacing a transparent one have been studied as a function of the fluid rheology and flow rate. The front width increases linearly with distance indicating a convection of the fluids with a low transverse mixing between the flow paths. The width also increases with the flow rate as the fluid rheology shifts from Newtonian at low shear rates towards a shear-thinning behaviour at higher shear rates. The width also increases with the polymer concentration at high flow rates. These results demonstrate the enhancement of the flow velocity contrasts between different flow channels for shear-thinning fluids. The relative widths at low and high shear rates for different polymer concentrations are well predicted by an analytical model considering the fracture as a set of parallel ducts of constant hydraulic apertures. The overall geometry of the experimental front geometry is also predicted by the theoretical model from the aperture map.

Keywords: Fractures; Dispersion; Shear thinning; Heterogeneity; Self-affine

1. Introduction

Transport and flow in porous media and fractured rocks are encountered in many engineering fields [1] and complex fluids such as polymer gels or surfactants are often involved. Applications include enhanced oil recovery (EOR), drilling muds and heavy oil recovery. In EOR, for instance, polymer flooding reduces viscosity-driven instabilities (a polymer solution is injected in the reservoir and followed by a water flood). When these complex fluids have shear-thinning properties, experimental flow measurements (see [2]) display specific features such as an enhancement of the effective hydraulic conductivity (or a reduction of the apparent viscosity) compared to the case of Newtonian fluids.

These effects may be strongly influenced by fractures which are frequently encountered in many reservoirs and generally display a broad range of characteristic length scales. While it is customary to visualize the fractures as parallel plates separated by a constant distance [3], this representation is rarely accurate: fracture wall surfaces are indeed rough and do not perfectly match [4]. This creates voids of various sizes resulting in spatial heterogeneities of the flow field [5,6].

The objective of the present work is to analyze experimentally and analytically the fluctuation of the flow velocity and its dependence on the fluid rheology and on the mean flow velocity for shear-thinning solutions flowing in transparent models of single fractures with rough walls. The experiments have been realized in a configuration in which flow is strongly channelized as is frequently the case in natural fractures [1]: this will be shown to allow for analytic predictions of the relation between the flow distribution and the apertures and, also, of their dependence on the rheological characteristics of the fluids used in the experiments.

We have sought particularly in this work to reproduce the roughness of natural fractured rocks which is characterized by a broad distribution of the characteristic length scales [7]. More

* Corresponding author. Tel.: +33 1 69 15 80 62; fax: +33 1 69 15 80 60.
E-mail address: hulin@fast.u-psud.fr (J.P. Hulin).

0377-0257/$ – see front matter © 2007 Elsevier B.V. All rights reserved.
doi:10.1016/j.jnnfm.2007.11.008

precisely, these surfaces can often be considered as *self-affine* [8], this means that they remain statistically invariant under the scaling transformation:

$$h(\lambda x, \lambda y) = \lambda^{\zeta} h(x, y), \tag{1}$$

where $h(x, y)$ is the surface height and ζ is the roughness or self-affine exponent. For most materials including granite, ζ is close to 0.8 [9] but it is close to 0.5 for materials such as sandstone and sintered glass beads [10,11]. Many experiments suggest that ζ is independent on the orientation of profiles measured on the surface with respect to the direction of crack propagation (a slight anisotropy has however been recently observed experimentally on some materials [12]).

The rough surfaces used in the present work are transparent milled plexiglas plates with an isotropic self-affine geometry of characteristic exponent $\zeta = 0.8$: they allow for optical flow observations by means of dyed fluids (practically, a transparent solution is displaced by a dyed one and the geometry of the front is determined by image analysis). For each fracture, two such complementary surfaces are realized and match perfectly when brought in contact: in the model, both a spacing normal to the mean fracture surface and a relative lateral shift $\vec{u}$ are introduced in order to create a mismatch and to obtain a variable aperture field [13].

While the surfaces are isotropic, previous laboratory measurements and numerical investigations [14–18] show that the lateral shift introduces an anisotropy of the permeability which is higher in the direction perpendicular to $\vec{u}$. More precisely, flow channels perpendicular to $\vec{u}$ and with a length similar to the model appear as shown in a previous work [19]. As a result, for flow perpendicular to $\vec{u}$, the overall geometry of the displacement front of a fluid by another of same rheological properties is well reproduced by modelling the fracture as a set of parallel ducts with an hydraulic aperture constant along the flow [19]: the present work deals exclusively with this configuration.

The fluids used here display at low shear rates ($\dot{\gamma} < \dot{\gamma}_0$) a "plateau" domain in which they behave as Newtonian fluids of constant viscosity η_0 while, at higher shear rates $\dot{\gamma} > \dot{\gamma}_0$, η decreases with $\dot{\gamma}$ following a power law of exponent $1 - n$. Comparing the velocity contrasts between the different flow paths in the two regimes allows one therefore to estimate the influence of the rheology since the velocity contrasts should be enhanced in the shear-thinning case. Finally, an analytical model predicting the influence of the parameters η_0, $\dot{\gamma}_0$ and n on the variation of the fluid velocity fluctuations with $\dot{\gamma}$ is derived and compared to experimental observations.

2. Experimental procedure

2.1. Characteristics of the model fracture

The model fracture is made of two complementary rough self-affine surfaces without contact points: both surfaces are obtained from a transparent material by means of a milling machine and their size is 85 mm ×171 mm. A detailed description of the procedure is given in [18]: a self-affine surface $h(x, y)$ is first generated numerically using the mid-point algorithm [20] with a self-affine exponent $\zeta = 0.8$ as observed in many materials [9]. A second surface, complementary from the first one, is generated and then shifted numerically parallel to its mean plane by 0.33 mm. The milling tool is computer controlled and a complex tortuous path may be imposed to obtain the self-affine geometry. Moreover, the borders of two parallel sides of the surfaces rise above the rough surface: they are designed so that, when clamped against the matching border of the other surface, there is a void space in the remaining area. The mean planes of the facing surfaces are parallel outside these borders with a mean distance: $\bar{e} = 0.77$ mm.

The local aperture $e(x, y)$ at a location (x, y) in the fracture plane may be predicted from the mathematical surface $h(x, y)$ by the relation:

$$e(x, y) = h(x, y) - h(x, y + u) + \bar{e}, \tag{2}$$

where u is the lateral shift. Fig. 1 shows the aperture field of the fracture considered in this work: the binarized image (lower part of Fig. 1) displays a clear anisotropy and a large correlation length perpendicular to the shift $\vec{u}$. Quantitatively, this effect may be characterized by the following correlation function, also called semivariance [21]:

$$\Gamma(\vec{\delta}) = \langle (e(\vec{r}) - e(\vec{r} + \vec{\delta}))^2 \rangle, \tag{3}$$

measuring the spatial correlation of the aperture field between two points separated by a lag vector $\vec{\delta}$. Orientations of $\vec{\delta}$ perpendicular (x-direction) and parallel (y-direction) to the shift are of

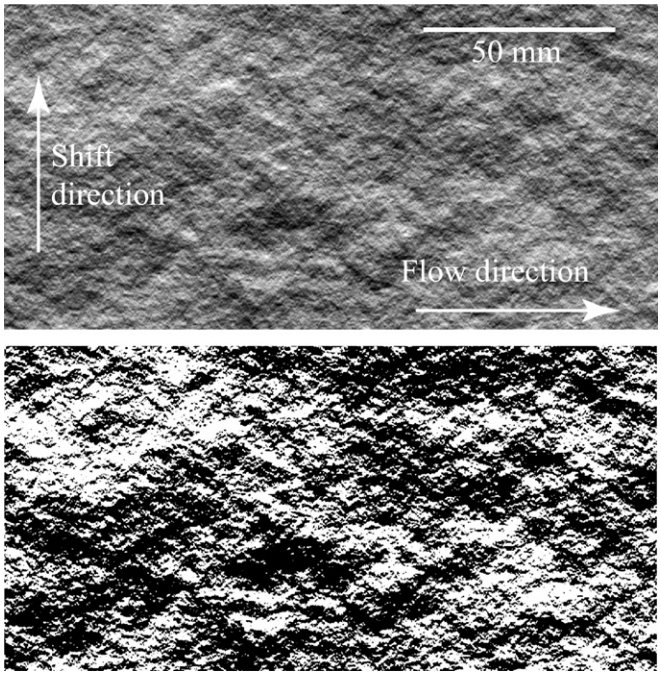

Fig. 1. Upper figure, gray scale representation of the aperture field. Field of view: 85 mm ×171 mm. Aperture field—mean value: $\bar{e} = \langle e(x, y) \rangle_{(x,y)} = 0.77$ mm; and the aperture fluctuation: $\sigma_e = \langle (e(x, y) - \bar{e})^2 \rangle_{(x,y)}^{1/2} = 0.1$ mm. Shift amplitude: $u = 0.33$ mm (oriented vertically on figure). In the present work, flow is parallel to x direction (horizontal on the figure). Lower image: binarized aperture field with a threshold value equal to the mean aperture (0.77 mm).

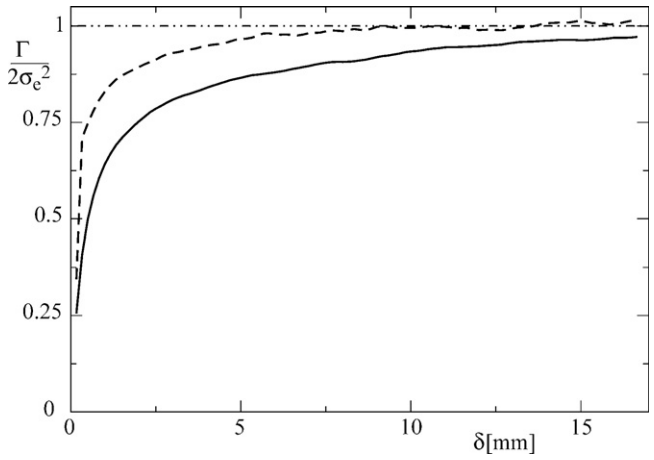

Fig. 2. Variation of the normalized semivariograms, $\Gamma/(2\sigma_e^2)$ as a function of lag distance $\|\vec{\delta}\|$ (mm) for the aperture field displayed in Fig. 1. Dotted line: correlation along the direction y of the shear. Solid line: correlation along the perpendicular direction x (parallel to the flow in the rest of the paper).

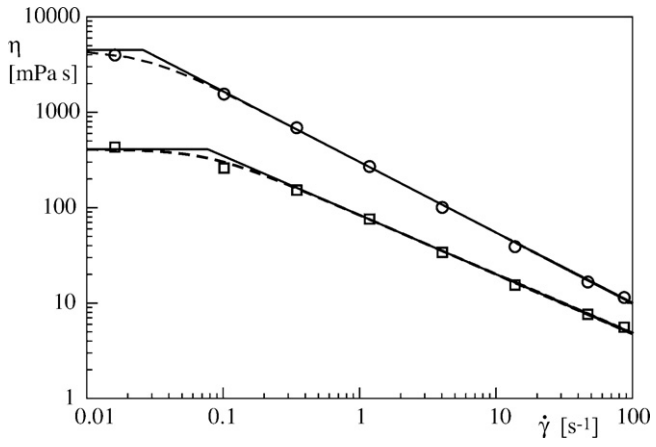

Fig. 3. Variation of the effective viscosity η of the polymer solutions as a function of the shear rate $\dot{\gamma}$ for two water-polymer solutions of different concentrations: 500 ppm (□) and 1000 ppm (◯). Dashed lines: Carreau functions corresponding to the sets of parameters of Table 1; continuous lines: truncated power law approximation corresponding to $a = \infty$ in Eq. (4).

special interest. Fig. 2 displays variations of the semivariance in both directions. When the lag modulus $\|\vec{\delta}\|$ is larger than the correlation length of the aperture field, one expects Γ to reach a constant value equal to $2\sigma_e^2$, where $\sigma_e^2 = \langle e(x, y) - \bar{e}\rangle^2$ is the variance of the aperture. The semivariance Γ reaches this limit, but in a very different way for the two orientations of $\vec{\delta}$. In the direction y parallel to the shift, Γ becomes of the order of (and sometimes larger than) $2\sigma_e^2$ for $\|\vec{\delta}\| > 8$ mm. In the perpendicular direction x, Γ never exceeds the saturation value and slowly increases towards it: these differences reflect the large-scale anisotropic structure of the aperture field. They can be characterized by defining a correlation length as the distance at which $\Gamma/(2\sigma_e^2)$ is equal to 0.5: this length is respectively of the order of 0.25 mm and 0.5 mm in the parallel and perpendicular directions.

Semivariograms have been computed on surface maps of epoxy casts of a fractured granite sample in a previous work [19] and display similar features: moreover, normalized curves $\Gamma/(2\sigma_e^2)$ corresponding to different values of u displayed a universal variation as a function of the normalized lag δ/u. This suggests that results obtained in the present work might be extrapolated to other values of u.

Finally it should be noted that the ratio S of the standard deviation of the aperture σ_e to the mean aperture $\bar{e}$ is only of 0.13 (Fig. 1). This implies, as discussed by [22], that the fracture can be considered as "hydraulically" smooth with relatively small velocity contrasts between and along flow lines. This keeps the trajectories of the preferential flow channels relatively straight and simplifies subsequent analysis.

2.2. Experimental set-up and procedures

The plexiglas model fracture is held vertically in a fixed position between a light panel and a 12-bit digital CCD camera with a high stability and dynamical range. Flow is induced by sucking a dyed solution from the topside while the lower side is slightly dipped into a bath containing a clear fluid. An appropriate calibration, described in Ref. [18], allows one to obtain from all pictures of each experiment the corresponding concentration map $c(x, y, t)$. Here, we focus on the geometry of the isoconcentration front $c/c_0 = 0.5$ which is determined by thresholding the concentration maps and which depends strongly on the heterogeneity of the flow field.

2.3. Rheological characteristics of shear-thinning solutions

In this work, we used shear-thinning polymer solutions, more specifically water–scleroglucan solutions; they have been characterized using a *Contraves LS30* Couette rheometer for shear rates $\dot{\gamma}$ ranging from 0.016 s^{-1} up to 87 s^{-1}. Two different polymer concentrations equal to 500 ppm and 1000 ppm have been used. The rheological properties of the dyed and transparent solutions have been verified to be constant with time within experimental error over 3 days; the variation of the effective viscosity η as a function of the shear rate $\dot{\gamma}$ is displayed in Fig. 3. The variation of η with $\dot{\gamma}$ is well adjusted by the Yasuda–Carreau function (dashed line):

$$\eta = \frac{1}{(1 + (\dot{\gamma}/\dot{\gamma}_0)^a)^{(1-n)/a}}(\eta_0 - \eta_\infty) + \eta_\infty. \quad (4)$$

The values of the corresponding rheological parameters for the polymer solutions characterized in the present work are listed in Table 1. η_∞ is too low to be determined within the available range of shear rates ($\dot{\gamma} \leq 87$ s^{-1}) and it has been taken equal to the viscosity of the solvent (*i.e.* water). In Eq. (4), $\dot{\gamma}_0$ corresponds to a crossover between two behaviours. On the one hand,

Table 1
Rheological parameters of scleroglucan solutions used in the flow experiments

Polymer concentration (ppm)	n	$\dot{\gamma}_0$ (s^{-1})	η_0 (mPa s)	a
1000	0.26±0.02	0.026±0.004	4490±400	2
500	0.38±0.04	0.077±0.02	410±40	2

for $\dot{\gamma} < \dot{\gamma}_0$, the viscosity η tends towards the limiting value η_0, and the fluid behaves as a Newtonian fluid. On the other hand, if $\dot{\gamma} > \dot{\gamma}_0$, the viscosity follows a power law variation reflecting its shear-thinning characteristics with $\eta \propto \dot{\gamma}^{(n-1)}$. For each experiment, the flow rate is kept constant at a value between 0.01 ml/min and 5 ml/min (corresponding mean flow velocities: $0.0003\,\mathrm{mm\,s^{-1}} \leq v \leq 0.14\,\mathrm{mm\,s^{-1}}$). Under such conditions, the typical shear rate at the surface of the fracture walls $\dot{\gamma} = 6v/\bar{e}$ (see Section 4.1) ranges between $2.5 \times 10^{-3}\,\mathrm{s^{-1}}$ and $1.1\,\mathrm{s^{-1}}$. The latter value is far below the shear rate corresponding to the second Newtonian plateau ($\eta = \eta_\infty$) and this limit will not be considered in this work. On the contrary, the lowest values of the typical shear rate are much lower than $\dot{\gamma}_0$: the Newtonian "plateau" in the rheological curves may therefore have a crucial influence of the flow properties.

In order to obtain a simple expression accounting for the effect of the fluid rheology on the velocity fluctuations, the rheological law of the fluids is approximated in Section 4 by a truncated power law which corresponds to the limiting form of Eq. (4) for $a = \infty$ (continuous line in Fig. 3). When $\dot{\gamma} < \dot{\gamma}_0$, the viscosity $\eta(\dot{\gamma})$ is considered as constant and equal to η_0; for $\dot{\gamma} > \dot{\gamma}_0$, $\eta(\dot{\gamma})$ is assumed to follow a power law $\eta(\dot{\gamma}) = m\dot{\gamma}^{n-1}$ in which $m = \eta_0/\dot{\gamma}_0^{n-1}$. The parameters n, $\dot{\gamma}_0$ and η_0 are obtained from Table 1. While this expression does not reproduce accurately viscosity variations in the transition zone, it captures well the essential features of the rheology of the fluid at low and high shear rates. Its key feature is to allow for analytical computations of the effect of the fluid rheology on the velocity fluctuations: this allowed us to demonstrate the enhancement of the channeling effects for shear-thinning solutions which is the topic of the present work.

3. Flow velocity dependence of front geometry

The distribution of the two fluids during the displacement depends significantly on the flow rate: this is observed clearly in Fig. 4 which displays three maps of the relative concentration C (in gray levels) corresponding to different flow rates (increasing from (a) to (c)) and to similar injected volumes (in all cases, the polymer concentration is equal to 1000 ppm). The geometry of the mixing zone will be characterized in the following by that of the displacement front (white lines) assumed here to coincide with the isoconcentration line $C(x, y, t) = 0.5$. Two important features of the displacement front have been observed: (a) its geometry depends on the flow rate Q and (b) its width parallel to the flow increases linearly with the distance from the injection side. The first point is illustrated by Fig. 4 which displays three isoconcentration fronts overlaid on the corresponding concentration maps and measured during fluid displacements at three different flow rates, but for a same polymer concentration (1000 ppm): the front width parallel to the flow direction is clearly larger at the highest flow rate.

The broadening of the displacement front may be characterized quantitatively from the variation of the mean square front width, $\sigma_x(t) = \langle (x(t) - \bar{x}(t))^2 \rangle^{1/2}$, as a function of the mean distance $\bar{x}(t)$ of the front from the injection side (Fig. 5). For all

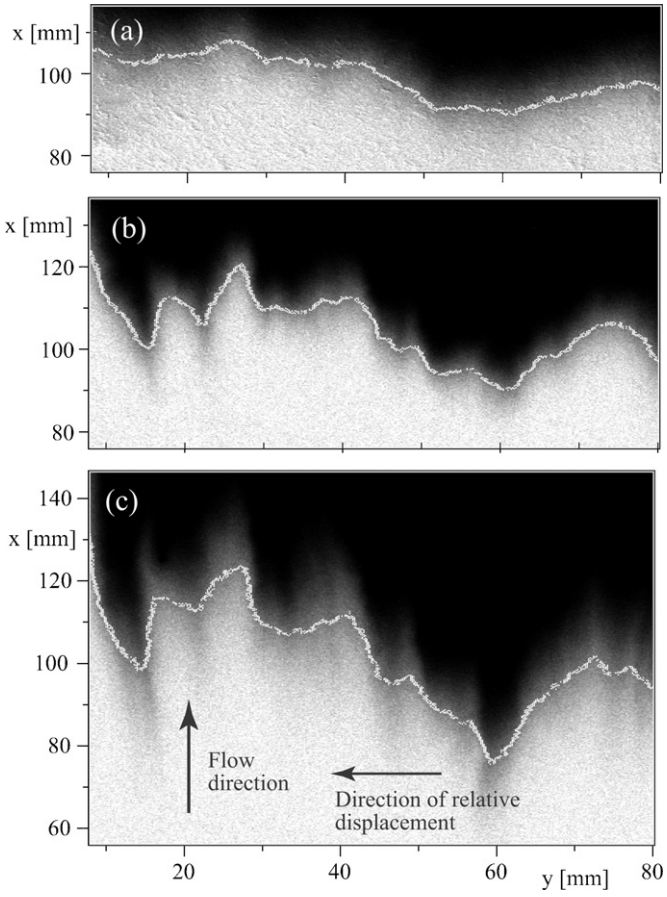

Fig. 4. Maps of the relative concentration $C(x, y, t)$ and corresponding displacement fronts (in white) at three different flow rates. (a) $Q = 0.01$ ml/min ($\bar{v}/v_c \simeq 1$); (b) $Q = 0.1$ ml/min ($\bar{v}/v_c \simeq 10$); (c) $Q = 1$ ml/min ($\bar{v}/v_c \simeq 100$). The velocity v_c corresponds to the transition between Newtonian-like ($v < v_c$) and shear-thinning ($v > v_c$) flows (see Section 4). Polymer concentration: 1000 ppm. Pure injected fluid appears in white and displaced fluid in black. x scale: distance from left side of model; y scale: distance from injection line. Correlation length of aperture field in the direction parallel (respectively perpendicular) to the flow (as defined in Section 2.1) = 0.5 (respectively) 0.25 mm; amplitude of the relative shift of the walls (see orientation on figure): $u = 0.33$ mm.

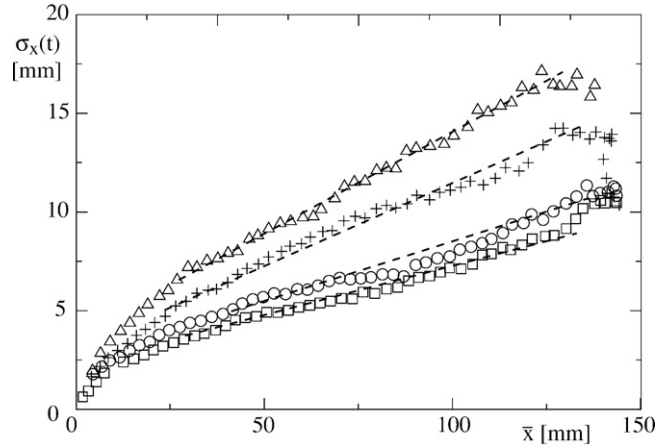

Fig. 5. Variation of the mean front width $\sigma_x(t) = \langle (x(t) - \bar{x}(t))^2 \rangle^{1/2}$ as a function of the mean distance $\bar{x}(t)$ from the inlet side of the model. Polymer concentration: 1000 ppm. Flow rates (Q): (△) 2.0 ml/min, (+) 0.5 ml/min, (◯) 0.1 ml/min, (□) 0.02 ml/min.

values of Q, $\sigma_x(t)$ increases linearly with $\bar{x}(t)$. In the next section, this will be shown to result directly from the underlying channelized structure of the aperture field. The width of the front after a transit time t corresponds then directly to the product $t\Delta v$ where Δv is the velocity difference between the different channels (the transverse exchange between channels is too small to allow one to reach a diffusive spreading regime).

At all distances, the width $\sigma_x(t)$ increases with the flow rate Q but with a particularly sharp variation between $Q = 0.1$ ml/min and 0.5 ml/min. It will be seen that, at this transition flow rate, the shear rate at the fracture walls becomes of the order of $\dot{\gamma}_0$ (the threshold value above which the fluids display shear-thinning characteristics).

4. Modelization

4.1. Flow between parallel plates with a constant gap

We compute the flow of the polymer solutions between parallel plates using the same approach as in Ref. [23]. The relation between the longitudinal pressure drop and the velocity profile in the gap is obtained by using the truncated power law model discussed in Section 2.3. The flow field is unidirectional and parallel to x so that $v_x(z)$ is the only non-zero velocity component. The strain rate is given by $\dot{\gamma}(z) = \mathrm{d}v_x/\mathrm{d}z$.

At low pressure gradients, the fluids behave like a Newtonian fluid with a constant viscosity η_0 and the resulting velocity profile is parabolic and symmetrical between the walls. Then, the shear rate is zero half way between the fracture walls and reaches a maximum at their surface where $\dot{\gamma} = 6v/e$ (e is the distance between the plates). This value of $\dot{\gamma}$ is proportional to the mean flow velocity or, equivalently, to the pressure drop.

As the flow rate keeps increasing, $\dot{\gamma}$ becomes larger than $\dot{\gamma}_0$ and the non-Newtonian characteristics of the fluid modify the velocity profile. The mean flow velocity v_c corresponding to the transition between the two regimes satisfies: $v_c = e\dot{\gamma}_0/6$ and the corresponding pressure gradient is $\nabla P_c 2\eta_0\dot{\gamma}_0/e$.

As v increases above v_c, the layer where the shear rate is higher than $\dot{\gamma}_0$ becomes thicker and the velocity profile $v_x(z)$ is no longer parabolic: the full expression may be derived analytically and is given in Eq. (5) of Ref. [23]. The mean velocity, v, can then be computed by integrating $v_x(z)$ over the fracture gap, leading to

$$v = \frac{e^2}{12(2n+1)\eta_0}\nabla P\left[(1-n)\left(\frac{\nabla P}{\nabla P_c}\right)^{-3} + 3n\left(\frac{\nabla P}{\nabla P_c}\right)^{(1-n)/n}\right]. \quad (5)$$

We consider now the case of shear-thinning fluids such that $n > 0$ and $(1-n)/n > -1$. Then, the leading term in Eq. (5) is $(\nabla P/\nabla P_c)^{(1-n)/n}$ and, therefore, when $\nabla P \gg \nabla P_c$, Eq. (5) becomes:

$$v \simeq \frac{e^2}{12}\left(\frac{\nabla P}{\eta_{\mathrm{eff}}}\right)^{1/n}, \quad (6)$$

where $\eta_{\mathrm{eff}} = \eta_0(2\dot{\gamma}_0/e)^{1-n}((2n+1)/3n)^n$. This is similar to the generalized version of Darcy's law often applied to the flow of non-Newtonian and, more specifically, to power law fluids in porous media [24–27].

4.2. Flow in rough fractures

In this part, we focus on the variations of the velocity in the plane (x, y) of the fracture and we assume therefore a two-dimensional flow field $\vec{v}(x, y)$ equal to the average of the fluid velocity profile over the gap with $\vec{v}(x, y) = \langle\vec{v}(x, y, z)\rangle_z$.

The development with time of the front (represented by the isoconcentration lines $c/c_0 = 0.5$) will now be analyzed by assuming that its points move at the local flow velocity $\vec{v}(x, y)$ and an analytical model predicting the global front width will be developed.

This model is based on the results of a previous work [19] demonstrating that, in such systems, the aperture field is structured into channels perpendicular to the lateral shift $\vec{u}$ of the surfaces. For a mean flow parallel to these channels, the paths of the tracer particles have a weak tortuosity; also, the velocity variations along these paths are small compared to the velocity contrasts between the different channels. Under these assumptions, the velocity of a particle located at a distance y, perpendicular to the mean velocity, satisfies:

$$\vec{v}(x, y) \approx v(y)\vec{e}_x, \quad (7)$$

where $\vec{e}_x$ is the unit vector parallel to the mean flow. Note also that, in the geometry discussed in this section, there are no contact points between the walls of the fractures: this avoids to take into account the large tortuosity of the flow lines in their vicinity.

If the fluid is Newtonian with a constant viscosity, then, for each channel, the velocity is related to the pressure gradient ∇P by relation (6) with $n = 1$; e is now an equivalent (or hydraulic) aperture associated to each channel and noted $e(y)$ and the equation represents the classical linear equivalent of Darcy's law for fractures. Previous studies have shown that, for relatively small aperture fluctuations, this hydraulic aperture is well approximated by the geometrical aperture [5,22]: this suggests that $e(y)^2$ can be taken equal to the mean of the average of the square of the local apertures along the direction x, *i.e.* $e(y)^2 = \langle e(x, y)^2\rangle_x$. The validity of this assumption has been tested numerically previously for a similar geometry [19] in the case of a Newtonian fluid: these simulations used the lattice Boltzmann method to determine the $2D$ front geometry at all times: except for fine scale details, the profile $x(y, t)$ of the distance of the front from the inlet at a given time t follows very closely the variations of $e(y)^2$.

For a power law fluid such that $n < 1$, the velocity satisfies the non-linear generalized relation (6). We seek now to generalize to this case the relation between the front geometry and the aperture variation established for the Newtonian fluids: the aperture field is still assumed to be strongly correlated in the flow direction, allowing one to consider the fracture as a set of parallel ducts.

We consider particles starting at $t = 0$ from the inlet of the model at different transverse distances y and moving at different

velocities $v(y)$. Then the distance x of the particles from the inlet at time t after the injection satisfies $x(y,t) = v(y)t$ so that the mean distance of the front from the inlet side is $\bar{x}(t) = \langle v(y)\rangle_y t = \bar{v}t$ and

$$\frac{x(y,t)}{\bar{x}(t)} = \frac{v(y)}{\bar{v}}. \tag{8}$$

Moreover, the mean square deviation $\sigma_x(t) = \langle (x(y,t) - \bar{x})^2 \rangle^{1/2}$ should satisfy: $\sigma_x(t) = \sigma_v t$ where σ_v is the mean square deviation of the velocities in individual channels from their mean value $\bar{v}$. Combining the previous relations leads to

$$\frac{\sigma_x(t)}{\bar{x}(t)} = \frac{\sigma_v}{\bar{v}}. \tag{9}$$

This equation shows that there is a direct relation between the front geometry and the variations of the velocity from one channel to another: for power law fluids, the latter are related to the variations of the hydraulic aperture by Eq. (6). In order to estimate these variations, we introduce a modified reduced aperture deviation S_h defined as the ratio between the standard deviation of the hydraulic aperture $e(y)$ to its mean. The parameter S_h is equivalent to the reduced aperture deviation S defined in Section 2.1 but the geometrical aperture is replaced by the hydraulic one. Here, we are interested in weakly fluctuating systems, *i.e.* for which both S and S_h are small compared to one. In addition, the hydraulic aperture $e(y)$ is observed to follow a Gaussian distribution. Moreover, Eq. (6) shows that, for a given pressure gradient ∇P, v scales as $e^{n+1/n}$: together with the above assumptions, this leads to the following relation between the reduced velocity fluctuations $\sigma_v/\bar{v}$ and S_h:

$$\frac{\sigma_v}{\bar{v}} = \frac{n+1}{n} S_h. \tag{10}$$

Combining Eqs. (9) and (10), leads to

$$\frac{\sigma_x(t)}{\bar{x}(t)} = \frac{n+1}{n} S_h. \tag{11}$$

5. Quantitative comparison between the experiments and the model

In the present experiments, the polymer solutions are expected to behave like Newtonian fluids as long as the shear rate $\dot{\gamma}$ is everywhere lower than the critical value $\dot{\gamma}_0$ (see Table 1). As the flow rate increases, the critical shear rate $\dot{\gamma}_0$ is first reached at the wall of the fracture where $\dot{\gamma}$ is highest. If the fracture is modeled as two parallel plates separated by the mean aperture $\bar{e}$, then $\dot{\gamma} = \dot{\gamma}_0$ at the walls when the mean flow velocity is $v_c = \bar{e}\dot{\gamma}_0/6$. Above this velocity, the shear-thinning properties of the fluids influence the flow and enhance the velocity fluctuations.

Fig. 6 displays the experimental variations of the normalized velocity fluctuations (equal to the normalized front width $\sigma_x(t)/\bar{x}(t)$) as a function of the reduced velocity $\bar{v}/v_c$ for both polymer solutions. The values predicted by Eq. (11) for a Newtonian fluid ($n = 1$) and for power law fluids with the same index as the two solutions are also plotted.

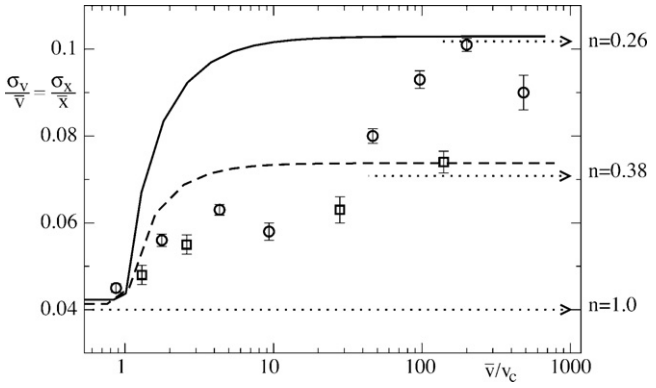

Fig. 6. Experimental variation of the ratio $\sigma_v/\bar{v} = \sigma_x/\bar{x}$ in the model fracture ($S_h \simeq 0.02$) as a function of the normalized mean velocity $\bar{v}/v_c$ for shear-thinning solutions of concentrations 1000 ppm (◯) and 500 ppm (□). Horizontal dotted lines: theoretical values of $\sigma_v/\bar{v}$ computed from Eq. (11) for a Newtonian fluid ($n = 1$) and for 500 ppm (respectively 1000 ppm) polymer solutions ($n = 0.38$, respectively 0.26). Solid and dashed lines: variations of $\sigma_v/\bar{v}$ as a function of $\bar{v}/v_c$ computed by integrating Eq. (5).

For $\bar{v}/v_c < 1$ the experimental values are similar for both solutions and close to the theoretical prediction for $n = 1$ (horizontal dashed line). For $\bar{v}/v_c \gg 1$, $\sigma_x(t)/\bar{x}$ tends toward values of the order of those predicted by Eq. (11) and increasing with the polymer concentration.

Eq. (11) provides therefore a good estimate of the velocity fluctuation inside the fracture both for low, *i.e.* $\bar{v}/v_c < 1$, and high flow rates corresponding to $\bar{v}/v_c \gg 1$. The increase of $\sigma_x(t)/\bar{x}$ between the Newtonian and shear-thinning regimes and also, at high velocities, with the polymer concentration confirms the enhancement of the velocity contrasts between the channels for shear-thinning fluids.

Between the limiting values $\bar{v}/v_c < 1$ and $\bar{v}/v_c \gg 1$, fluid velocity variations within the fracture may be estimated by applying Eq. (5) to each channel (assumed to be of constant hydraulic aperture): this equation takes into account the coexistence in the fracture gap of layers where the fluid has Newtonian and non-Newtonian properties. The normalized velocity fluctuations $\sigma_v/\bar{v}$ obtained by this computation are displayed in Fig. 6 for the two polymer concentrations together with the experimental variations of the normalized front width $\sigma_x(t)/\bar{x}(t)$.

In agreement with the theoretical curves, $\sigma_x(t)/\bar{x}(t)$ starts to increase when the velocity $\bar{v}$ becomes larger than v_c ($\bar{v}/v_c > 1$) for both polymer solutions. However, although the limiting value for $\bar{v}/v_c \gg 1$ is the same as predicted, the increase of $\sigma_x(t)/\bar{x}(t)$ above v_c is slower than expected: actually, the theoretical predictions represent an upper bound for the observations.

This difference may be due in part to the use of a simplified model of the rheological curve which displays a sharper transition than the actual one between the Newtonian and shear-thinning regimes: this will, in turn, smoothen the variation of $\sigma_x/\bar{x}$. Numerical computations using $a = 2$ instead of $a = \infty$ in Eq. (4) will be necessary to estimate the magnitude of this effect. Also, the aperture of the parallel channels introduced in the model is assumed to be constant: this also leads to a transition between the Newtonian and power law regimes which is faster than the actual one.

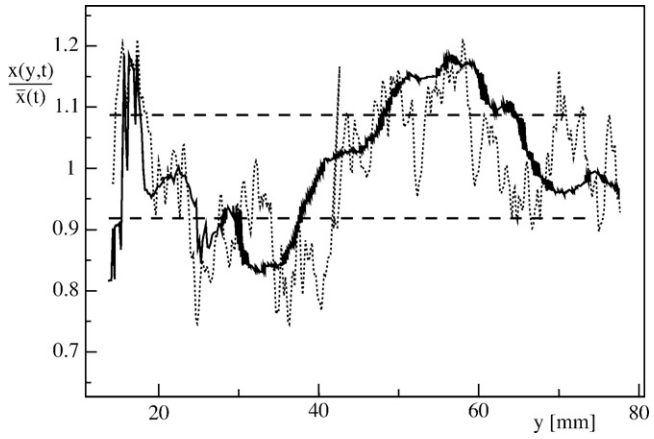

Fig. 7. Thick solid line: experimental normalized front profile $x(y,t)/\bar{x}(t)$ as a function of the transverse distance y (mm) for $\bar{v}/v_c = 200$ for a 1000 ppm shear-thinning polymer solution. Dotted line: theoretical variation of the normalized velocity $v(y)/\bar{v}$ in the parallel flow channel model. The front is displayed just before the displacing fluid starts to flow out of the fracture. Dashed lines: characteristic deviations of the distance $x(y)$ from its mean value $\bar{x}$.

A step further in the interpretation is the comparison of the experimental shape of the fronts with that estimated from the channel model. In Section 4.2, the normalized distance $x(y,t)/\bar{x}(t)$ of the front from the inlet has been predicted to be equal to $v(y)/\bar{v}$ (see Eq. 8). An experimental front profile normalized in this way is plotted in Fig. 7 as a function of the transverse distance y together with the variation of the theoretical normalized velocity $v(y)/\bar{v}$. The velocity $v(y)$ is estimated from Eq. (6) in which the aperture e is replaced by the mean value $e(y)$ defined in Section 4.2.

The most remarkable observation is the fact that both the experimental and theoretical fronts have not only the same width but also nearly the same geometry. These results are very similar to those of numerical simulations for Newtonian fluids [19]: they demonstrate the validity of the generalization in Eq. (6) to non-Newtonian fluid. Fine scale details predicted by the theoretical model are however not observed in the experimental front: this difference may be due in part to viscous drag forces between parallel layers of fluid moving at different velocities in the fracture plane. These forces may smoothen the local velocity gradients and rub out small-scale features of the front without changing the large-scale velocity variations: this results in a bumpy front with a typical width of the structures of the order of 10 mm. This latter value is of the order of the correlation length in the direction perpendicular to the channels.

6. Discussion and conclusions

In the present work, the enhancement of velocity fluctuations for shear-thinning fluids has been studied in a single fracture with rough, self-affine walls. The two wall surfaces are perfectly matched and are positioned with both a normal and a lateral shift. This results in an anisotropic aperture field well characterized quantitatively by the semivariograms of the aperture both in the direction of the shift and perpendicular to it. The characteristics of these semivariograms are in agreement with previous experimental measurements on granite samples [19]. Parallel to the shift, the correlation length of the aperture field (as defined is Section 2.1) is equal to 0.25 mm and the correlation cancels out (*i.e.* $\Gamma/(2\sigma_a^2)$ becomes equal to 1) at a distance of the order of 10 mm. In the other direction, the correlation length is higher (0.5 mm) and some correlation subsists over the full fracture length.

This observation has allowed us to model the fracture as a set of parallel ducts perpendicular to the shift and with an hydraulic aperture constant along their length. These assumptions lead to specific predictions on the dependence of the width and of the geometry of the front on the velocity of the fluid and its rheology: these predictions deal with the case of a mean flow parallel to the channels which was the configuration used in the present experiments. This model generalizes a previous one developed for Newtonian fluids and which has been validated by numerical simulations [19].

The variation of the front width with the velocity could first be predicted. At low flow rates, the viscosity of the solutions is constant (Newtonian "plateau") but non-Newtonian effects become important for faster flows: this results in an increase of the velocity fluctuations—and of the front width. This variation occurs when the shear rate at the fracture wall becomes larger $\dot{\gamma}_0$, *i.e.* the shear rate corresponding to the crossover between the Newtonian plateau and the power law regimes: $\dot{\gamma}_0$ is reached for a mean flow velocity $v_c = \bar{e}\dot{\gamma}_0/6$. At still higher flow velocities of the order of $100v_c$, both the normalized velocity fluctuations and the normalized front width reach a new constant value with a good agreement between the experimental results and the theoretical expectations.

These results validate the prediction of an enhancement of velocity contrasts for shear-thinning channelized flows in fractures. The experimental increase of the front width with the mean velocity v right above the threshold value v_c is however slower than the predictions. The origin of this discrepancy might be investigated by using a more refined theory taking into account both the full rheological characteristics of the fluid (in the present work, the rheology is approximated by a truncated power law) and the aperture variations along the flow.

Another possible origin of the difference is viscoelasticity effects. These are related to the value of the Deborah number defined as the ratio between the typical relaxation time of the polymer λ and a time characterizing the flow field. For a dilute polymer solution, the relaxation time τ may be estimated as the inverse of the value of the shear rate $\dot{\gamma}_0$ corresponding to the upper limit of the Newtonian plateau. This leads to respective values $\tau = 38$ s and 13 s for the 1000 ppm and 500 ppm solutions (a relaxation time $\tau \simeq 10$ s of the same order of magnitude, although lower, has been obtained for 1000 ppm scleroglucan solutions from G' and G'' measurements [28]). In the present geometry, the characteristic time associated to the flow field may be taken equal to the transit time over the correlation length of the aperture in the direction the flow: this length has been taken equal in Section 2.1 to the value $\delta_c \simeq 0.5$ mm of the lag distance for which the normalized correlation function $\Gamma/(2\sigma_e^2)$ is equal to 0.5 (See Fig. 2). Note that this length is also of the order of magnitude of the shear displacement ($u = 0.33$ mm).

The Deborah number is therefore taken equal to $De = v/\dot{\gamma}_0\delta_c$ in which v is the mean fluid velocity. The relation $v_c = \dot{\gamma}_0\bar{e}/6$ leads then to $De \sim (\bar{e}/(6\delta_c)(v/v_c))$ or $De \sim 0.25v/v_c$. In the present work, the ratio v/v_c ranges from 1 to 300 so that De is larger than 1, except at the lowest flow rates: viscoelastic effects may therefore be important. As a result, the adjustment to aperture variations along the flow of the fluid velocity profiles (and more specifically of the fraction of the aperture corresponding to a shear-thinning behaviour) may be incomplete. The spatial fluctuations of the apparent viscosity (and therefore of the velocity) will then be smaller than expected from the model.

The theoretical model also allows one to predict the geometry of the experimental front down to length scales of the order of 10 mm. Future work should investigate the influence of transverse velocity gradients on the shape of the front for different types of fluids.

The results obtained in the present work demonstrate therefore clearly that approaches developed to analyze channelized Newtonian flows in fractures can be generalized to non-Newtonian fluids and allow to predict, for instance, the variation of the velocity contrasts with the rheology.

Numerical studies in $2D$ networks [26,27] had similarly shown that the flow of shear-thinning fluids is localized in a smaller number of preferential paths than for Newtonian ones. It has been suggested that these effects might account for the enhancement of the effective hydraulic conductivity for such fluids mentioned in Section 1: the results obtained in the present paper may therefore be usefully applicable to the numerical simulation of non-Newtonian flows in fracture networks.

A number of questions remain however open and need to be considered in future studies. First, in the models used here, the roughness of the fracture surface is smaller than the mean aperture width: this corresponds for instance to the propagation of a hydraulic fracture when its aperture is kept large compared to the roughness by the hydraulic pressure. The results will however not be valid in the frequent cases in which contact points are present in the fracture [29].

Then, the present experiments have been realized with a mean flow parallel to the channels created by the relative shift of the wall surfaces. It will be important to compare these results with the case of flow perpendicular to these channels: velocity fluctuations in the directions parallel and perpendicular to the flow should then be significantly different from those in the present experiments. Eq. (5) should, for instance, be modified.

Finally, this work deals with relatively short path lengths such that transverse exchange between channels may be considered as negligible: the results obtained may therefore be different for longer path lengths. It is also possible that the spatial correlation of the velocity field will eventually decay at very long distances, although this has not been observed in our experimental model.

Acknowledgements

We are indebted to G. Chauvin and R. Pidoux for their assistance in the realization of the experimental set-up. This work was funded by E.E.C. through the STREP Pilot plant program SES6-CI-2003-502706 and by the CNRS-PNRH program. This research was also supported by a CNRS-CONICET Collaborative Research Grant (PICS CNRS 2178), by the ECOS A03-E02 program and by the I029 UBACyT programs.

References

[1] N.R. Council (Ed.), Rock Fractures and Fluid Flow: Contemporary Understanding and Applications, National Academy Press, Washington, DC, 1996.
[2] C. Perrin, P. Tardy, K. Sorbie, J. Crawshaw, Experimental and modeling study of Newtonian and non-Newtonian fluid flow in pore network micromodels, J. Colloid Interf. Sci. 295 (2006) 542–550.
[3] J. Bodin, F. Delay, G. de Marsily, Solute transport in a single fracture with negligible matrix permeability. 1. Fundamental mechanisms, Hydrogeol. J. 11 (2003) 418–433.
[4] B. Vickers, S. Neuman, M. Sully, D. Evans, Reconstruction and geostatistical analysis of multiscale fracture apertures in a large block of welded tuff, Geophys. Res. Lett. 19 (1992) 1029–1032.
[5] S. Brown, Fluid flow through rock joints: the effect of surface roughness, J. Geophys. Res. 92 (1987) 1337–1348.
[6] Y. Tsang, C. Tsang, Flow channeling in a single fracture as a two-dimensional strongly heterogeneous permeable medium, Water Resour. Res. 25 (1989) 2076–2080.
[7] C. Poon, R. Sayles, T. Jones, Surface measurement and fractal characterization of naturally fractured rocks, J. Phys. D: Appl. Phys. 25 (1992) 1269–1275.
[8] B. Mandelbrot, Self-affine fractals and fractal dimension, Phys. Scripta 32 (1985) 257–260.
[9] E. Bouchaud, The morphology of fracture surfaces: a tool for understanding crack propagation in complex materials, Surf. Rev. Lett. 10 (2003) 797–814.
[10] J.M. Boffa, C. Allain, J.P. Hulin, Experimental analysis of fracture rugosity in granular and compact rocks, Eur. Phys. J. Appl. Phys. 2 (1998) 281–289.
[11] L. Ponson, H. Auradou, P. Vie, J.-P. Hulin, Low self-affine exponents of fracture surfaces of glass ceramics, Phys. Rev. Lett. 97 (2006) 125501.
[12] L. Ponson, D. Bonamy, H. Auradou, G. Mourot, S. Morel, E. Bouchaud, C. Guillot, J. Hulin, Anisotropic self-affine properties of experimental fracture surfaces, Int. J. Frac. 140 (2006) 27–36.
[13] S.R. Brown, R.L. Kranz, B.P. Bonner, Correlation between the surfaces of natural rock joints, Geophys. Res. Lett. 13 (1986) 1430–1433.
[14] S. Gentier, E. Lamontagne, G. Archambault, J. Riss, Anisotropy of flow in a fracture undergoing shear and its relationship to the direction of shearing and injection pressure, Int. J. Rock Mech. Miner. Sci. Geomech. Abstr. 34 (1997), 412–412.
[15] I. Yeo, M.D. Freitas, R. Zimmerman, Effect of shear displacement on the aperture and permeability of a rock fracture, Int. J. Rock Mech. Min. Sci. 35 (1998) 1051–1070.
[16] G. Drazer, H. Auradou, J. Koplik, J.P. Hulin, Self-affine fronts in self-affine fractures: large and small-scale structure, Phys. Rev. Lett. 92 (2004) 014501.
[17] H. Auradou, G. Drazer, J.P. Hulin, J. Koplik, Permeability anisotropy induced by a shear displacement of rough fractured walls, Water Resour. Res. 40 (2005) W09423.
[18] A. Boschan, H. Auradou, I. Ippolito, R. Chertcoff, J. Hulin, Miscible displacement fronts of shear thinning fluids inside rough fractures, Water Resour. Res. 43 (2007) W03438.
[19] H. Auradou, G. Drazer, A. Boschan, J.P. Hulin, J. Koplik, Flow channeling in a single fracture induced by shear displacement, Geothermics 35 (2006) 576–588.
[20] R. Voss, Fundamental Algorithms in Computer Graphics, Springer-Verlag, Berlin, 1985, p. 805.
[21] P. Kitanidis, Introduction to Geostatistics: Applications in Hydrogeology, Cambridge University Press, Cambridge, UK, 1997.

[22] R. Zimmerman, S. Kumar, G. Bodvarsson, Lubrification theory analysis of the permeability of rough-walled fractures, Int. J. Rock Mech. Min. Sci. Geomech. Abstr. 28 (1991) 325–331.
[23] S. Gabbanelli, G. Drazer, J. Koplik, Lattice Boltzmann method for non-Newtonian (power-law) fluids, Phys. Rev. E 72 (2005) 046312.
[24] M. Balhoff, K. Thompson, A macroscopic model for shear-thinning flow in packed beds based on network modeling, Chem. Eng. Sci. 61 (2006) 698–719.
[25] X. Lopez, P.H. Valvatne, M.J. Blunt, Predictive network modeling of single-phase non-Newtonian flow in porous media, J. Colloid Interf. Sci. 264 (2003) 256–265.
[26] C. Shah, Y. Yortsos, Aspects of flow of power law fluids in porous media, AIChE J. 41 (1995) 1099–1112.
[27] A. Fadili, P. Tardy, A. Pearson, A 3D filtration law for power-law fluids in heterogeneous porous media, J. Non-Newton. Fluid Mech. 106 (2002) 121–146.
[28] J.S. Paschkewitz, C.D. Dimitropoulos, Y.X. Hou, V.S.R. Somandepalli, M.G. Mungal, E.S.G. Shaqfeh, P. Moin, An experimental and numerical investigation of drag reduction in a turbulent boundary layer using a rigid rodlike polymer, Phys. Fluids 17 (2005) 085101.
[29] L.J. Pyrak-Nolte, N.G.W. Cook, D.D. Nolte, Fluid percolation through single fractures, Geophys. Res. Lett. 15 (1988) 1247–1250.